LA-UR--85-1396

DE85 010748

TITLE. THE LOS ALAMOS SPHEROMAK PROGRAM

AUTHOR(S): S(tephen) O. Knox, Cris W. Barnes, J(uan) C. Fernandez, I(vars) Henins, H(iroshi) W. Hoida, P(hillip) L. Klingner, D(avid) A. Platts, A(rthur) R. Sherwood, B(radford) L. Wright, T(homas) R. Jarboe, CTR-5; R(ulon) K. Linford, CTR-DO; G(eorge) Marklin, A(nthony) G. Sgro, CTR-6

SUBMITTED TO Dr. Manual Berrondo, Chairman
Plasma Physics Workshop, April 22-26, 1985
Instituto de Fisica
Universidad Nacional Autonoma de Mexico
Cuernavaca, Mexico

DISCLAIMER

Los Alamos National Laboratory
Los Alamos, New Mexico 87545

FORM NO. 836 R4
ST. NO. 2629 5/81

THE LOS ALAMOS SPHERCMAK PROGRAM

presented by Stephen O. Knox

T. R. Jarboe, C. W. Barnes, J. C. Fernandez, I. Henins, H. W. Hoida,
P. L. Klingner, S. O. Knox, R. K. Linford, G. Marklin,
D. A. Platts, A. G. Sgro, A. R. Sherwood, B. L. Wright

LOS ALAMOS NATIONAL LABORATORY
Los Alamos, New Mexico, 87545 U.S.A.

I. Introduction

The Los Alamos Spheromak Program consists of two experimental facilities. The confinement physics of sustained and decaying spheromaks are being studied in CTX, which has an extensive array of diagnostics. Experiments are directed towards extending the physics understanding of the spheromak as a magnetic confinement concept. Electrodes for the production of clean sustained spheromaks are developed or the Electrode Facility, which is more flexible in terms of experimental modifications. Improvements to helicity sources and electrodes which are proven on the Electrode Facility are then considered for incorporation onto CTX.

II. Magnetic Helicity

Spheromaks can be sustained against resistive decay by helicity injection because they tend to obey the minimum energy principle. This principle states that a plasma-laden magnetic configuration will relax to a state of minimum energy subject to the constraint that the magnetic helicity (which is a measure of the number of flux linkages) is conserved. The descriptive equation for the ideal equilibrium with force-free fields is $\nabla \times \vec{B} = \lambda \vec{B}$ with $\lambda \equiv \mu_0 j/B$ = constant. The units of λ are m^{-1}, and it is the ratio of magnetic energy to magnetic helicity for the configuration. The use of helicity as a constraint on the minimization of energy was first proposed by Woltjer[1] in connection with astrophysical phenomena. Helicity conservation was first applied to the spheromak by Wells and Norwood.[2] The principle was later applied to the reversed-field pinch (RFP) by Taylor,[3] who was most responsible for the eventual acceptance and recognition of the principle as being important for RFP-type confinement devices. Of course, helicity does decay on the resistive diffusion time. However, if helicity is created and made to

flow continuously into a confinement geometry, these additional linked fluxes can relax and sustain the configuration indefinitely against the resistive decay.

Magnetic helicity has traditionally been defined as a global quantity applicable to configurations of closed magnetic fields:

$$K = \int \vec{A} \cdot \vec{B} dV \quad (1)$$

with $\vec{B} \cdot \vec{n} = 0$ at the boundary of the volume in question. In this form, and in conjunction with the Taylor principle, this concept has had great utility in generating bounded equilibrium states. Difficulties can arise, however, when attempts are made to reduce the concept to more local terms, such as by defining a helicity density or a helicity flux. Helicity injection schemes for which $\vec{B} \cdot \vec{n} \neq 0$ can also present a problem. The central difficulty is that the artificial character of the vector potential, $\vec{A}$, makes manipulation of helicity sensitive to the choice of gauge. Indeed, if we apply the gauge transformation $\vec{A}' = \vec{A} + \nabla u$, it is readily shown from the above definition that

$$K' - K = \int u \vec{B} \cdot \vec{n} dS \quad (2)$$

so that for a generalized volume with $\vec{B} \cdot \vec{n} \neq 0$ over some region of its surface, the magnetic helicity is not well determined.

In the simple geometry of the CTX experiment, this rather technical theoretical issue is avoided by a direct approach. As illustrated by Moffatt[1], in the case of two separate, linked fluxes, ψ_1, and ψ_2, the above definition reduces to $K = 2\psi_1\psi_2$. In the CTX coaxial source, the poloidal and toroidal fields are separate with the poloidal flux ψ_s being generated by a coil and the rate of change of the toroidal flux being given by the source voltage V_s. The result is the rule $dK/dt = 2\psi_s V_s$ for the helicity injection rate which has been confirmed to our satisfaction by CTX data.

The gauge problem that arises in less elementary cases has been studied independently by a number of workers[4 - 6], as well as by persons at Los Alamos. The results of these studies indicate that the issue of generalized helicity is now essentially resolved. The interested reader is referred to

Refs. [4 - 6] for a complete analytic treatment of the guage-invariant problem.

For experimentalists, the concepts of field and flux often have more appeal than that of vector potential. In terms of these quantities, helicity can be thought of as a linkage of flux with flux and for a closed volume can be defined as

$$K = \int_0^{\psi_t} \psi_\ell d\psi \tag{6}$$

where ψ_ℓ is the amount of flux linking the incremental closed flux tube $d\psi$ and ψ_t indicates that integral is performed on all flux tubes within the closed volume of interest.

III. Efficiency of Helicity Injection

As one might expect, the energy per unit helicity as given by the parameter λ is a useful concept in discussing efficiency. The inverse of λ, λ^{-1}, can be thought of as the size of the magnetic structure. When fields relax they form the largest magnetic structure possible, subject to the boundary conditions and the conservation of helicity. Helicity therefore appears to move to regions of larger characteristic size. To achieve helicity flow from a source to the spheromak, the source must be physically smaller (or have a larger λ-parameter) than the spheromak. However if the source has a λ-parameter much larger than that of the spheromak, it will be very energy inefficient. Since helicity is conserved, the mismatch in λ-parameters is equal to the difference in energy leaving the source and the energy assimilated by the spheromak. This difference in energy values represents losses inherent to the relaxation process. Losses from this mismatch can be minimized by making the j/B of the source only slightly greater than that of the spheromak. Another energy loss in the electrode sustained spheromak is the ohmic dissipation in the field lines that contact the electrodes. Losses here are minimized by keeping low the fraction of spheromak flux which contacts the electrodes.

IV. Confinement Studies on CTX

In the CTX experiment, spheromak formation, sustainment and confinement studies have continued with a 140-cm-diameter mesh flux conserver (MFC) replacing an 80-cm-diameter MFC while still using the same coaxial helicity source. High temperatures (> 100 eV) were previously obtained for decaying spheromaks in the smaller flux conserver because the rapid particle loss ($\tau_p \cong 0.17$ ms) led to effective removal of impurity ions and because operation was achieved at high current densities.[7] Particle confinement in the larger flux conserver is significantly improved. We are no longer in a regime in which the particle loss time is short in comparison with the magnetic energy decay time of the spheromak. Impurity ions are not rapidly removed and it has therefore become important to improve the effectiveness of ohmic heating as represented by j/n, the ratio of current density to plasma density. Figure 1 shows the behavior of the plasma density and toroidal plasma current that is observed when the spheromak is formed in the larger MFC. A new mode of circuit operation has led to an improvement in the j/n ratio (to values $1 - 1.5 \times 10^{-14}$ A- m). In this mode, a long-pulse current waveform is obtained (by using pulse-forming networks with different pulse widths) with a slower risetime than that of the previous mode.[7,8] In addition, the source voltage is firmly clamped to zero (at 0.85 ms) so as to shut off the flow of plasma and impurities from the source electrode during the decay phase.

Multipoint Thomson scattering is used to measure the electron temperature. Figure 2 shows the central (average of seven points taken from r = 35 to 55 cm.) temperature. The average temperature begins to increase after the sustainment phase and in about 0.7 ms reaches a value of about 80 eV. It then decreases as the configuration continues to resistively decay.

The 140-cm-diameter MFC is equipped with about 40 Rogowski loops that measure the induced image currents in the MFC. By fitting the current pattern to an equilibrium code[9] we can deduce the internal magnetic field structure[10]. We have determined that λ is not a constant, but $\lambda(\psi)$, where ψ is the normalized poloidal flux function of the spheromak. Thus far, we have used a linear function for $\lambda(\psi)$ which is sufficient to establish the equilibrium and provide information on stability. The magnetic field profiles inferred from determining $\lambda(\psi)$ can then be analyzed in a stability code to find the most unstable kink modes.

Observations with the Rogowski loops reveal a rotating internal kink mode, with toroidal mode numbers n = 1,2,3 and 4 at different phases of the discharge. Figure 3 gives representative MFC currents as measured by the Rogowski loops. Since the spheromak equilibrium field is only poloidal at the outer surface, the toroidal Rogowski loops (measuring toroidal MFC currents) measure equilibrium plus oscillatory fields, and the poloidal loops (measuring poloidal MFC currents) measure only the oscillatory fields of the rotating internal kink mode.

Figure 4 shows linear $\lambda(\psi)$ fits to the Rogowski loop data at four different times during a representative shot which developed an n = 1 mode (characteristic of the sustainment phase), and then sucessive n = 2 and n = 3 modes during the decay phase. The circles of Fig. 4(a) are the experimental values for the toroidal hoop currents (normalized to hoop 5), and the solid lines of Fig. 4(a) are the theoretical MFC toroidal hoop current distributions for the best choice of α, where α is the slope of the linear $\lambda(\psi)$ function. Using the value for α, the corresponding $\lambda(\psi)$ and $q(\psi)$ for the equilibria are then calculated and shown in Figs. 4(b) and (c), respectively. During the formation phase (.1-.7 ms), the $\lambda(\psi)$-profile [c.f. Fig. 4(b)] is peaked towards the outside of the configuration ($\psi \to 0$), indicating a relatively high value of j/B in that region. This is consistent with the interpretation of spheromak sustainment using a coaxial source where currents are driven primarily on the outer flux surfaces. The next time interval is one where no oscillations are present (.8-1.05 ms). The $\lambda(\psi)$-profile is essentially independent of ψ ($\lambda(\psi)$=constant). This is the only time when the equilibrium is near the minimum energy or Taylor state. The spheromak does not remain in this transient state, nor does it return during the remainder of the resistive decay phase of the plasma. During the following time interval (1.1-1.4 ms), the the $\lambda(\psi)$-profile has changed slope and resistivity gradients cause j/B peaking towards the magnetic axis ($\psi \to 1$), resulting in a drop in q, the inverse rotational transform. The peaking continues during the next time interval (1.45-1.55 ms), where the $\lambda(\psi)$ slope increases even further. The configuration then terminates in this discharge when the particle density goes to zero. Notice that the q on axis is close to one when the n = 1 oscillation is observed, and close to 1/2 and 1/3 when the n = 2 and n = 3 oscillations are seen. The n = 3 mode is seen most clearly in association with a sudden termination that can occur under prescribed experimental conditions when the

density to magnetic field ratio, n/B, goes to zero. One interesting feature shown in Fig. 4 is that the $\lambda(\psi)$ and the corresponding q profile can be considerably different than the minimum energy state.

Figure 5 shows the (a) front, (b) back, (c) side and (d) top views of the surface current pattern measured for a rotating n = 2 mode. A set of 49 basis functions was used in the reconstruction. The effect of the entrance region on the front-back symmetry of the modes is quite apparent.

A new diagnostic on the CTX experiment is a multichord CO_2 interferometer [Fig. 6] that views the equatorial plane of the spheromak. It is designed for simultaneous use of eight beams, with the first (beam 1) intersecting the geometric or symmetry axis (r = 0) and successive beams (2 through 8) passing along chords roughly 7.7 cm apart. Beam 5 is approximately tangent to the magnetic axis. Beams 6 and 8 have just become active because their vacuum ports were previously occupied by other diagnostics. Inversion of data from the six beams yeilds density profile information as six concentric toroidal rings of constant density, centered about the symmetry axis. The time dependence of these six toroidal rings is given in Fig. 7, where the plasma density profile changes between sustainment (t = 0 - .85 ms) and decay (t > .85 ms). During the decay phase the density is seen to decrease on the outer flux surfaces (r = 5 cm) and increase towards the magnetic axis (r = 40 cm). These changes in the density profile show a general correspondence with the evolution of the current profile $\lambda(\psi)$, seen with the Rogowski loop array. In the transition interval between sustained and decaying phases, a "pumpout" phenomenon is seen in which a significant increase in density occurs within ring 1 (actually a 17-cm-diameter circle) at the symmetry axis. This phenomenon is accompanied by a density reduction in the adjacent regions represented by rings 2 and 3 but does not extend to the magnetic axis. The data of Fig. 7 have been low-pass filtered (f < 5 kHz) to reduce the amplitude of density fluctuations. We are studying the possibility of correlation between these fluctuations and the modes seen with the MFC Rogwoski loops. Using this diagnostic for n(r), the Rogowski loop data to infer j(r), and multipoint Thomson scattering for T(r) we are studying $V_{drift}/V_{thermal}$ ($\propto j/n\sqrt{T_e}$) as a function of time and position. Results of this study are still preliminary and will be reported at a later date.

V. Electrode Development

In the electrode studies facility the goal is to develop electrodes which can be used to cleanly sustain a steady state spheromak. The first experiments are aimed at testing some new geometries that might make better helicity sources than the present coaxial source. Some of the geometries employed have been tests of the generalized helicity injection concept, and the results have increased our confidence in the validity of the concept.

A new geometry now being tested is called the kinked Z-pinch source. If we imagine the entrance region of our coaxial source geometry to be an extended cylinder, the lowest energy state with finite helicity and no net axial flux is not an $m = 0$ azimuthally symmetric state, but one which is a helically-deformed $m = 1$ configuration. In spite of the coaxial geometry of the CTX source it is therefore possible that a nonsymmetric distribution of current enters the flux conserver. The question has been raised whether this tendency could be taken to its limit: an entrance region with two linked, helical fluxes side by side that are driven by a source with $m = 1$ symmetry. Figure 8 shows the kink Z-pinch source which should create the $m = 1$ structure. The cylindrical entrance region is terminated by a tee section with coils and electrodes for establishing a magnetized Z-pinch, which generates helicity. As the current is raised and the discharge becomes kink unstable, helicity should flow via the two helical flux tubes of the kink through the entrance region into the flux conserver. This flow is promoted by design[11], in that the pinch, entrance, and spheromak regions are associated with successively smaller values of λ. Magnetic field lines intersecting the pinch electrodes connect naturally with the $m = 1$ helical state in the entrance region. Connection between the entrance region and the spheromak is not fully understood, but presumably involves the introduction of one helical flux tube component along the geometric axis while the other flux tube maps onto the returning poloidal field at the flux conserver boundary. We are now studying this geometry and have confirmed that the source does make a spheromak. Figure 9 shows the radial magnetic fields profiles of a spheromak produced by this source, while Figure 10 shows the magnetic fields as a function of time.

Presently it appears that the helicity absorption efficiency and the impedance of the source are not much different from the coaxial source. However in evaluating various helicity injection schemes, the value of dK/dt

achieved is not the only basis for comparison. Given two sources of equivalent helicity injection capability, the determination of which is preferable depends on physics and technology issues. By physics issues we mean those aspects of source operation that affect the stability and transport of the spheromak. Technology issues relate more to source engineering, for example: the ease with which the source magnetic flux and current can be supplied; requirements for vacuum seals and insulating gaps; erosion and cooling requirements of electrode surfaces; and the structure which the helicity source presents to the neutron and energy fluxes of a fusion plasma. In comparison with the coaxial sources presently used, some technical advantages of the Z-pinch design are immediately apparent. The coaxial sources require a re-entrant center electrode with an internal solenoid. The amount of source flux that can be provided by this solenoid is undesirably restricted by space and cooling limitations. In the Z-pinch source, the magnetizing coils are external and this restriction on ψ_s can be relaxed. Greater flexibility is also seen for the design of the electrode surfaces. This should allow for a more extended and uniform distribution of current with concomitant improvements in impurity control. Another consequence of electrode decoupling is that, as seen by the spheromak, the helicity source becomes more nearly a simple hole in the flux conserver wall. At present, the technical advantages alone are sufficient for us to test this new source. It should also be noted among technical advantages that a kinked Z-pinch source, if feasible, could ultimately be operated without electrodes at all. This would be the case if a toroidal Z-pinch were used.

VI. Summary

We have discussed the concept of helicity and how it is being utilized in the spheromak program at Los Alamos. Physics experiments on CTX are directed towards understanding the confinement properties of the spheromak. In a separate facility (Electrode Facility), new sources of magnetic helicity are being explored. New source electrodes which can be used to cleanly sustain a steady-state spheromak are also being developed. A new helicity source, the kinked Z-pinch, which may be an improvement over coaxial sources, was discussed.

REFERENCES

[1] L. Woltjer, Proc. Nat. Acad. Sci. 44 (1958) 489.

[2] D. R. Wells and J. Norwood Jr., J. Plasma Physics 3 (1969) 21. E. E. Nolting, P. E. Jindra, and D. R. Wells, J. Plasma Physics 9 (1973) 1.

[3] J. B. Taylor, Phys. Rev. Letts. 33 (1974) 1139.

[4] J. H. Hammer, "Reconnection in Spheromak Formation and Sustainment," reprint from Magnetic Reconnection in Space and Laboratory Plasmas (1984)

[5] Torkil H. Jensen and Ming S. Chu, Physics. Fluids 27 (1984), 2881.

[6] M. A. Berger and G. B. Field, J. Fluid Mech. 147 (1984) 133-148.

[7] T. R. Jarboe, Cris W. Barnes, I. Henins, H. W. Hoida, S. O. Knox, R. K. Linford, and A. R. Sherwood, "The Ohmic Heating of a Spheromak to 100 eV," Phys. Fluids 27 (1) 13-15, 1984.

[8] Cris W. Barnes, T. R. Jarboe, I. Henins, A. R. Sherwood, S. O. Knox, Rita Gribble, H. W. Hoida, P. L. Klingner, C. G. Lilliequist, R. K. Linford, D. A. Platts, and R. L. Spencer, "Spheromak Formation and Operation with Background Filling Gas and a Solid Flux Conserver in CTX," Nuclear Fusion 24, 267 (1984).

[9] G. Marklin, "Numerical Models of CTX Equilibrium," paper presented at US/Japan Compact Toroid Workshop, November 10-15, 1984.

[10] S. O. Knox, Cris W. Barnes, G. Marklin, T. R. Jarboe, I. Henins, H. W. Hoida and B. L. Wright (submitted to Phys. Rev. Lett.).

[11] T. R. Jarboe, Cris W. Barnes, D. A. Platts, B. L. Wright, "A Kinked Z-Pinch as the Helicity Source for Spheromak Generation and Sustainment," to be published in Comments on Plasma Physics.

Figure Captions

1) Density and toroidal current vs. time for a typical CTX discharge.

2) CTX core temperature (35 - 55 cm average) vs. time from Thomson scattering.

3) Examples of Rogowski loop signals for a discharge which developed n = 1,2, and 3 modes during different phases of the discharge. The corresponding equilibria are given in Figure 4.

4) (a) Experimental values (circles) and theoretical MFC toroidal hoop current distributions (solid lines) during different phases of the discharge of Fig. 3.; (b) $\lambda(\psi)$ vs. ψ profiles for (a); (c) $q(\psi)$ vs. ψ profiles for (a). The times given in (a) are the intervals over which signals such as those in Fig. 3 were averaged in order to give the experimental values.

5) Surface current pattern of the n = 2 mode.

6) Schematic of the 8-chord CO_2 electron density interferometer.

7) Electron density vs. time a various radii as deduced from multi-chord interferometry.

8) Schematic of a new kinked Z-pinch helicity source.

9) Magnetic field profiles of a spheromak produced by the kinked Z-pinch source.

10) Magnetic field vs. time and density vs. time of a spheromak produced by the kinked Z-pinch source.

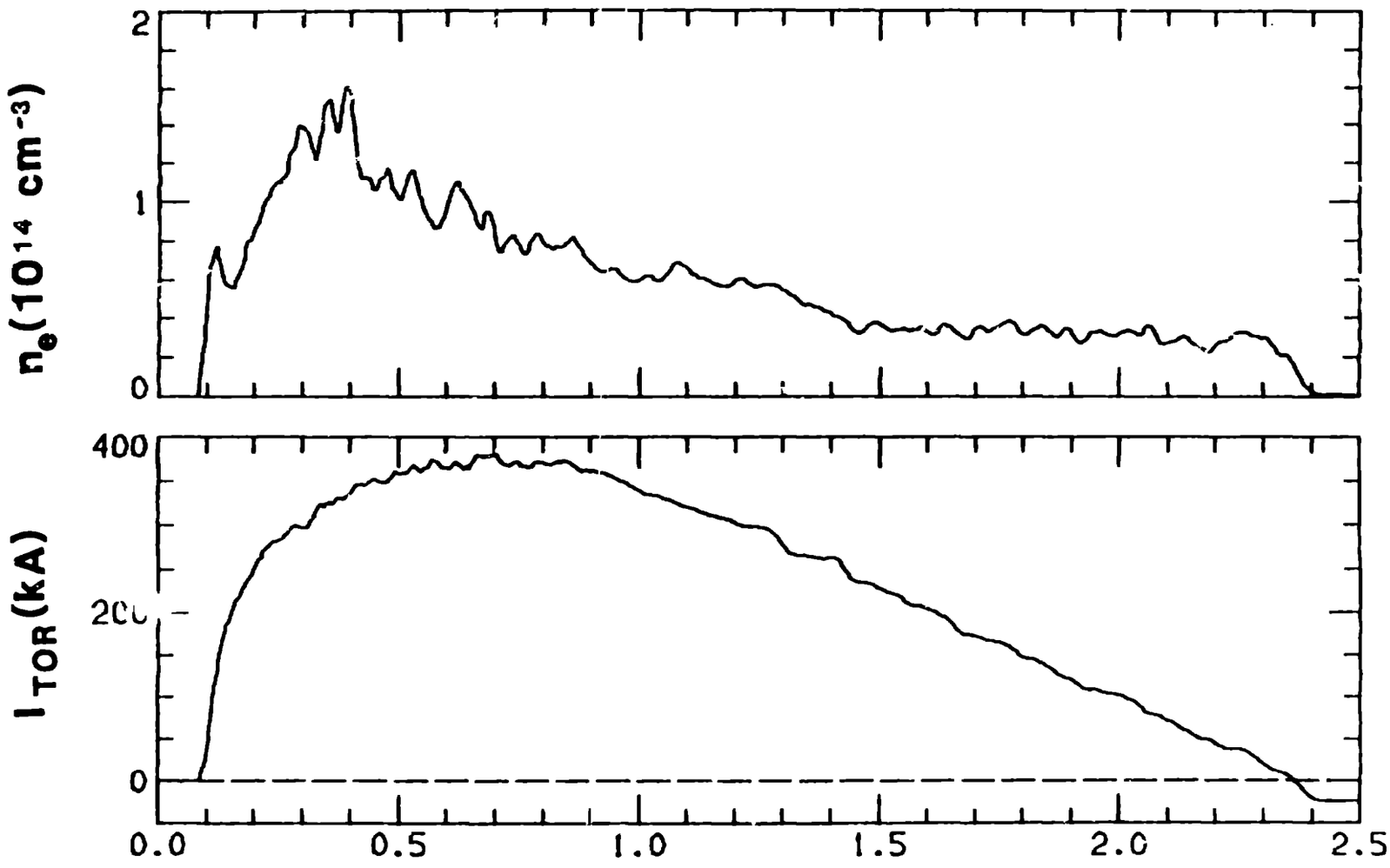

Figure 1

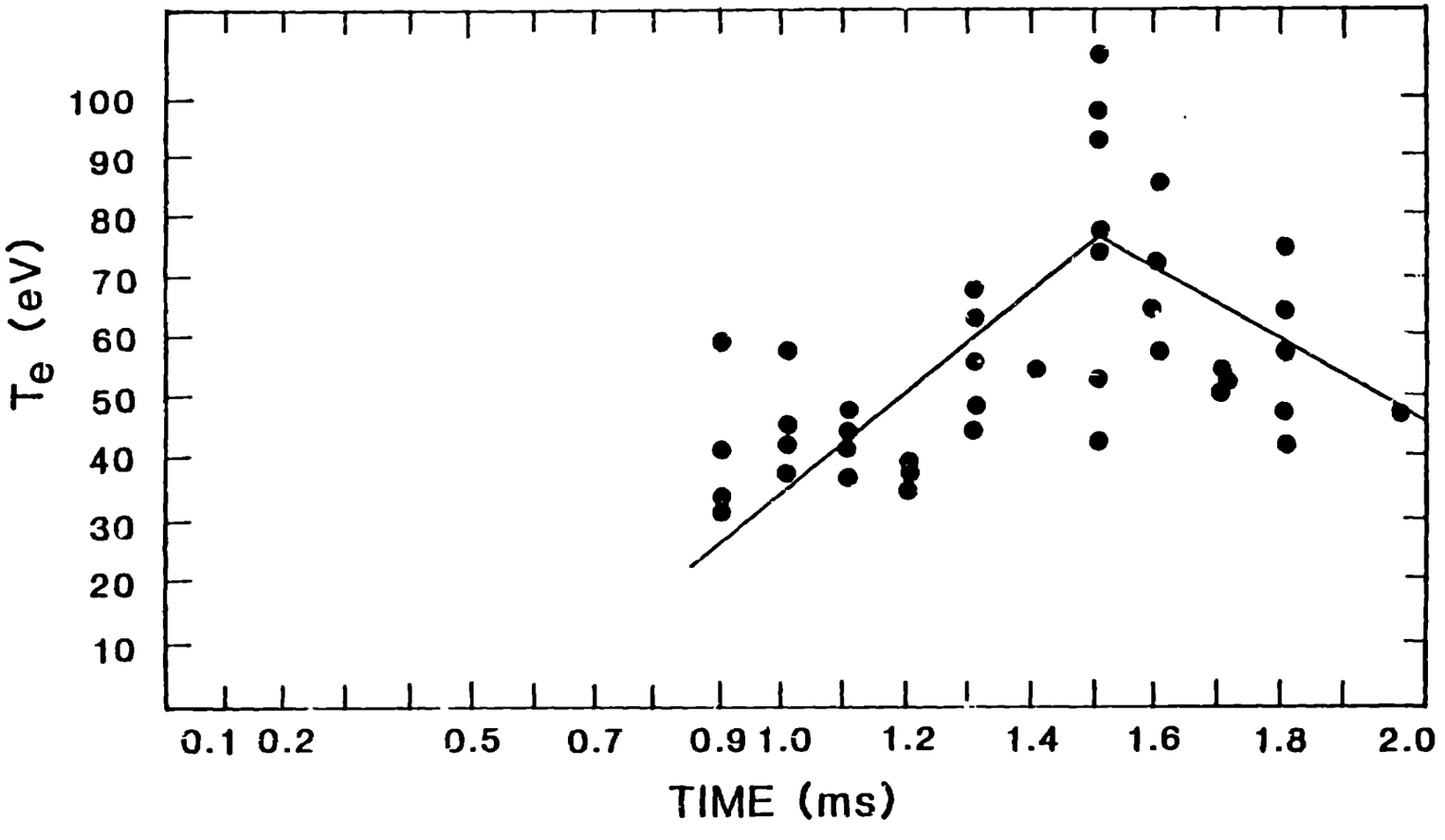
100
90
80
70
60
50
40
30
20
10
T_e (eV)
0.1 0.2 0.5 0.7 0.9 1.0 1.2 1.4 1.6 1.8 2.0
TIME (ms)

Figure 2

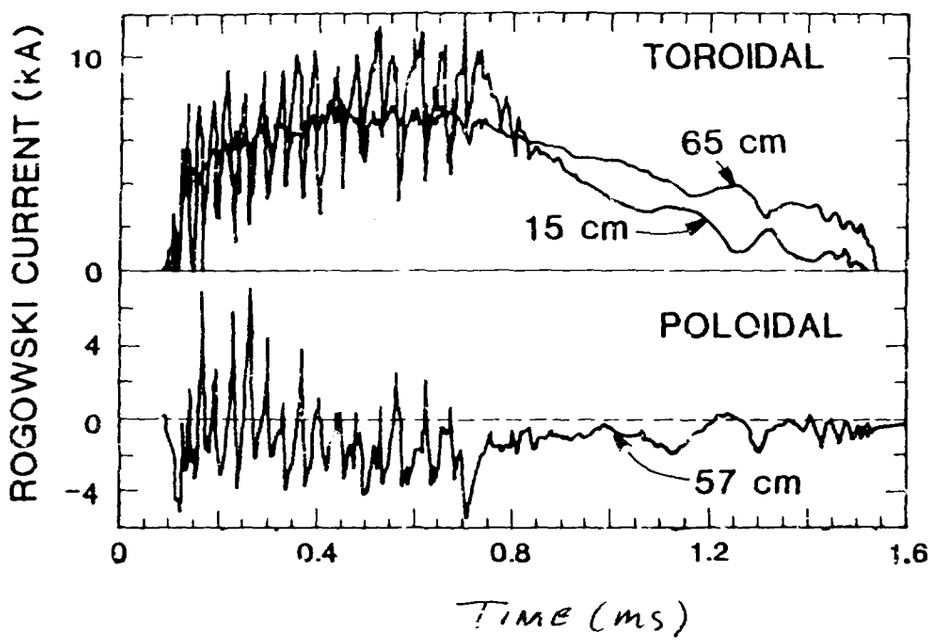
ROGOWSKI CURRENT (kA)
10
0
TOROIDAL
65 cm
15 cm
4
0
-4
POLOIDAL
57 cm
0
0.4
0.8
1.2
1.6
TIME (ms)

Figure 3

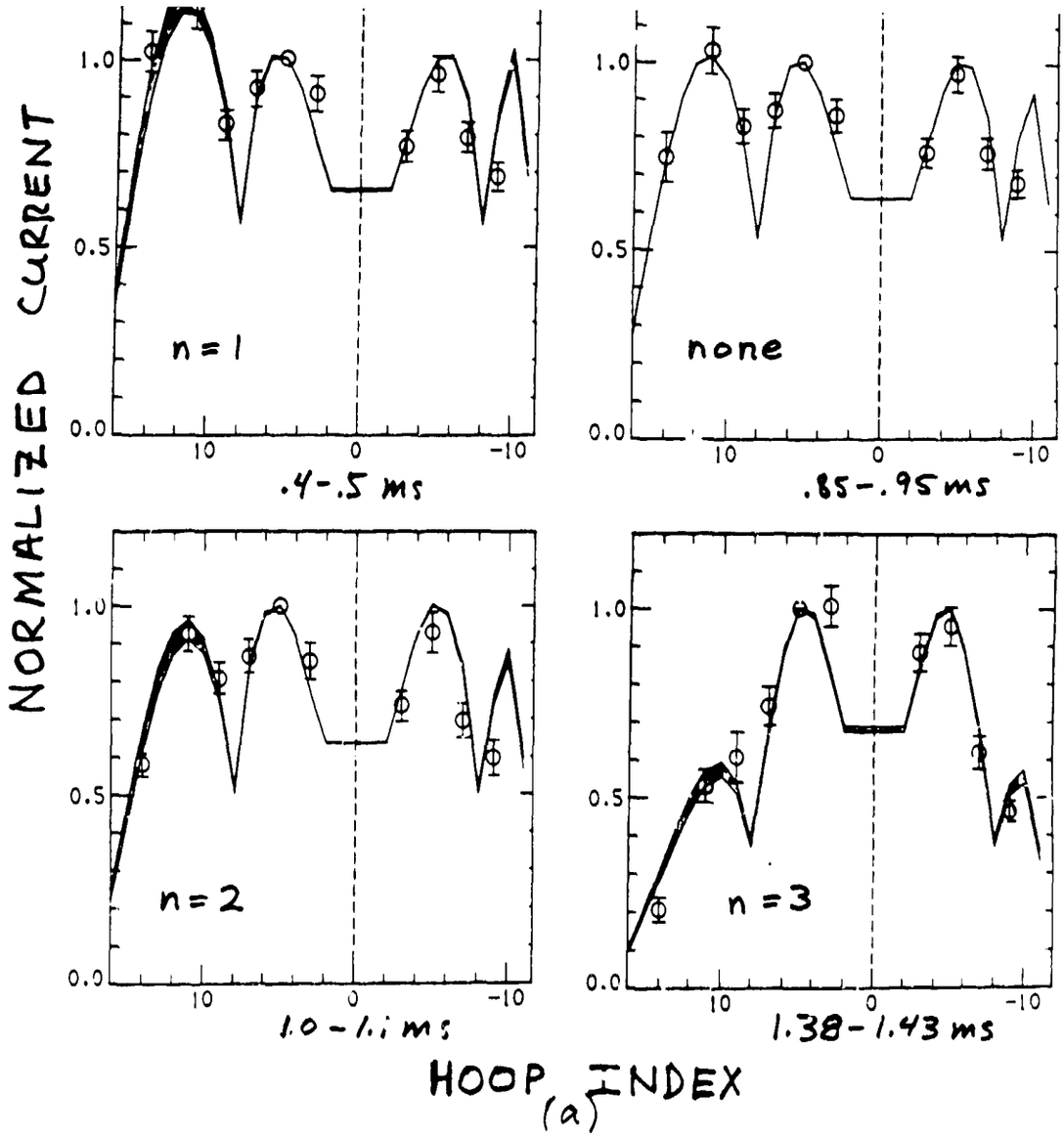
NORMALIZED CURRENT
n = 1
.4-.5 ms
none
.85-.95 ms
n = 2
1.0-1.1 ms
n = 3
1.38-1.43 ms
HOOP INDEX
(a)

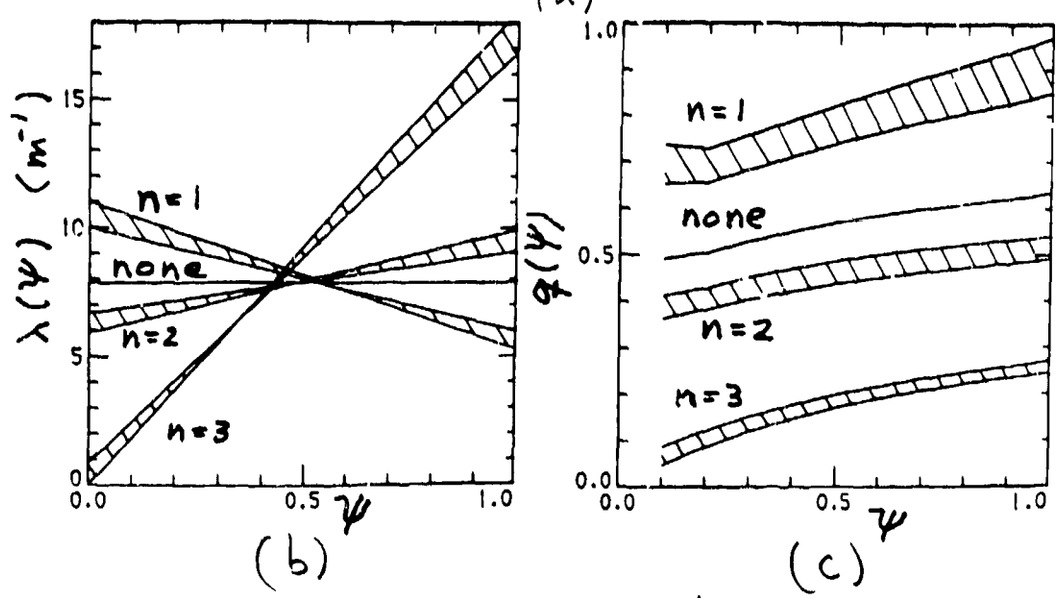
λ(ψ) (m⁻¹)
n=1
none
n=2
n=3
ψ
(b)
q(ψ)
n=1
none
n=2
n=3
ψ
(c)

Figure 4

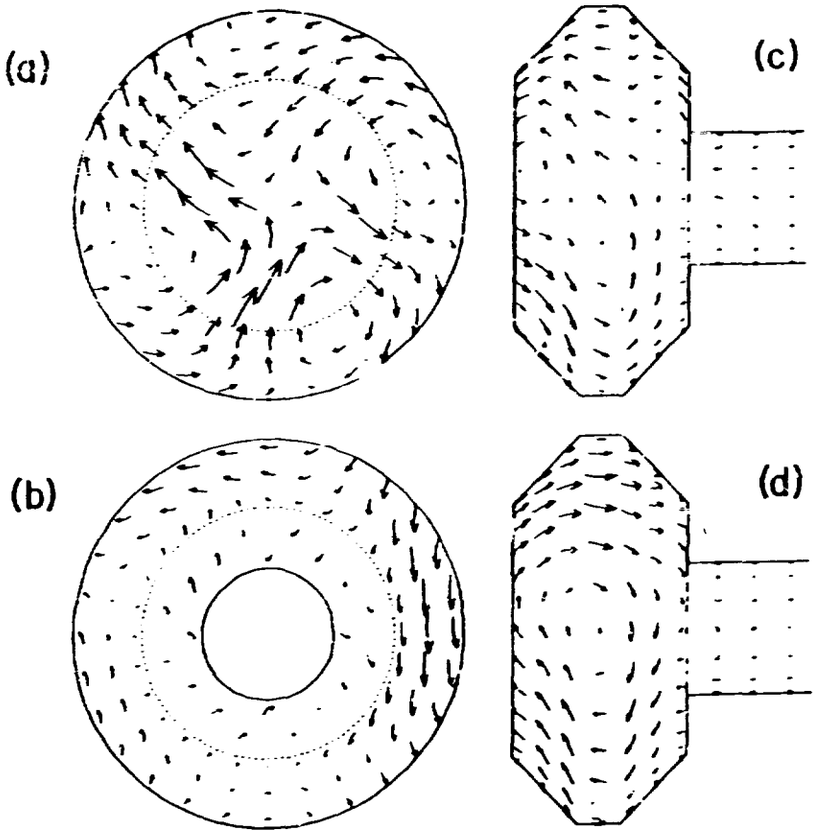

Figure 5

EIGHT-CHORD INFRARED INTERFEROMETER FOR THE CTX EXPERIMENT

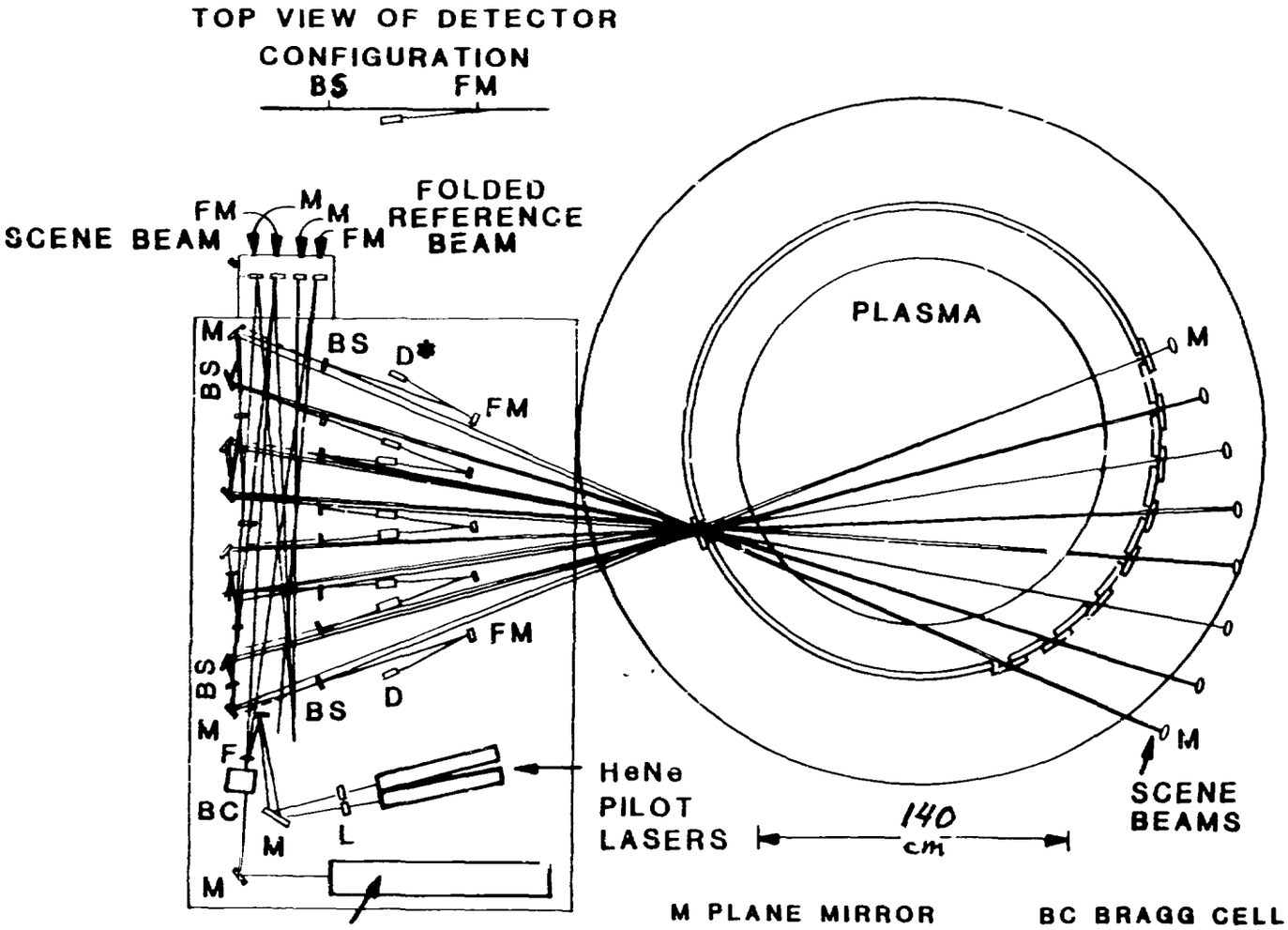

10/84ctr5562

Figure 6

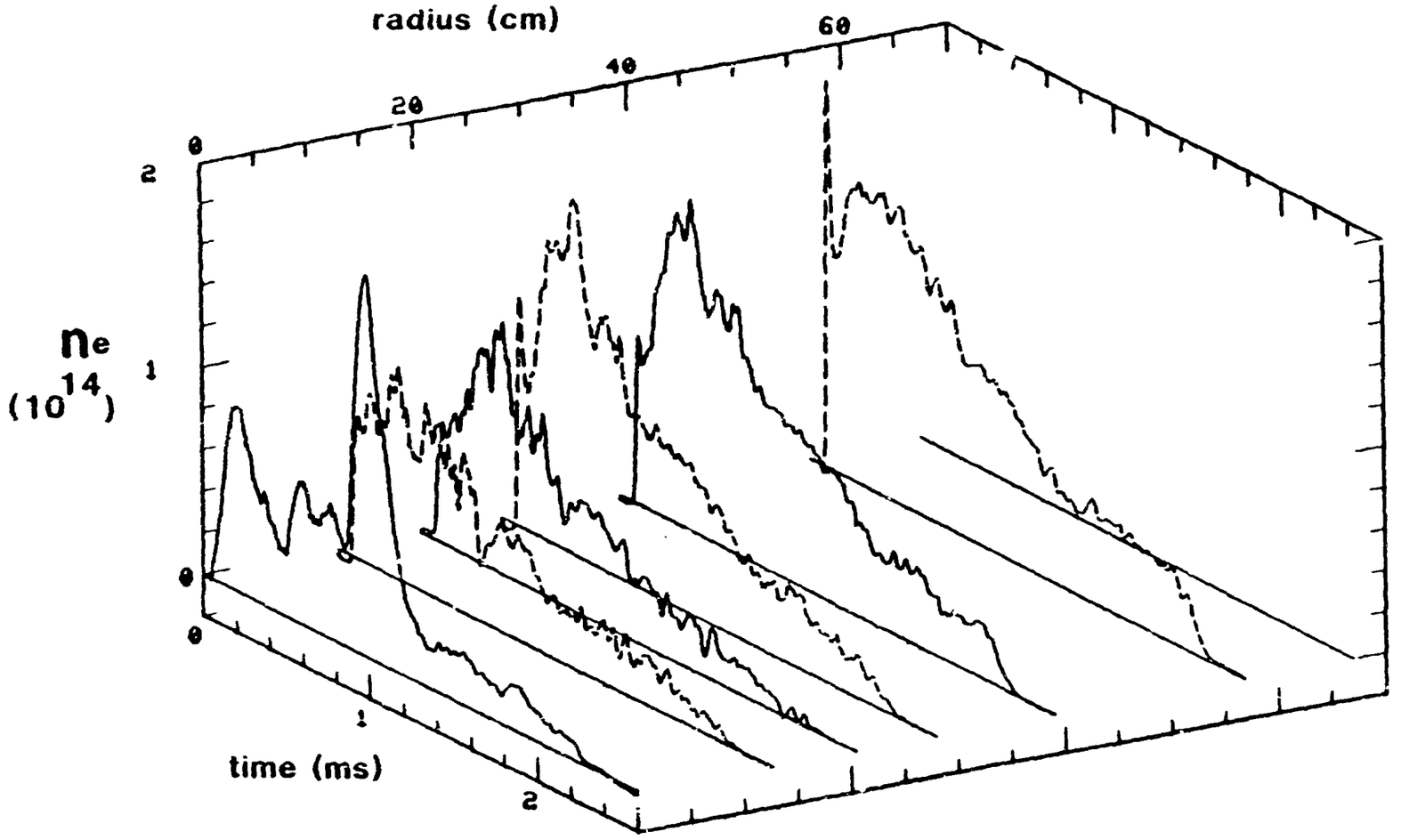

Figure 7

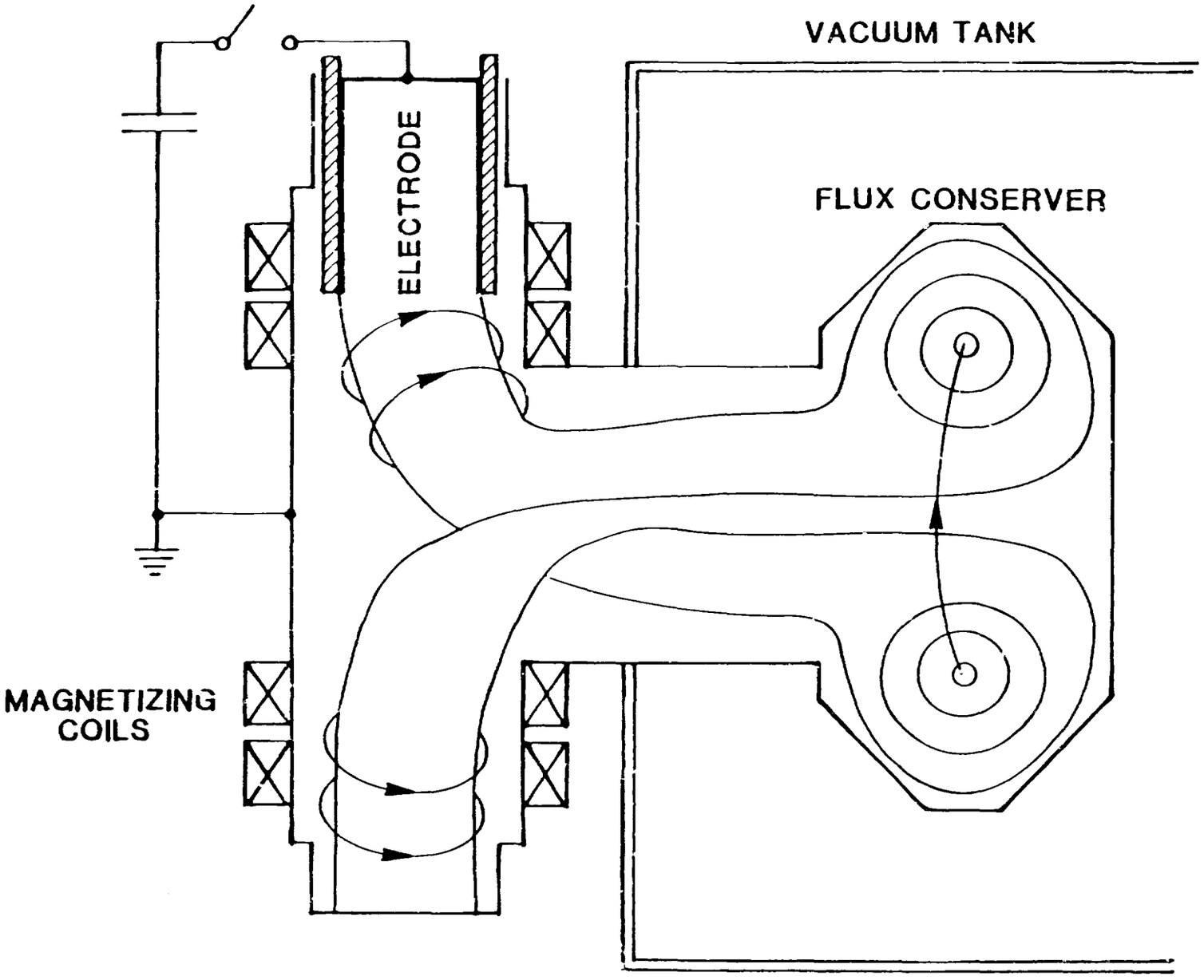

KINKED Z-PINCH HELICITY SOURCE

Figure 8

1/85 c1r5

KINKED Z-PINCH HELICITY SOURCE

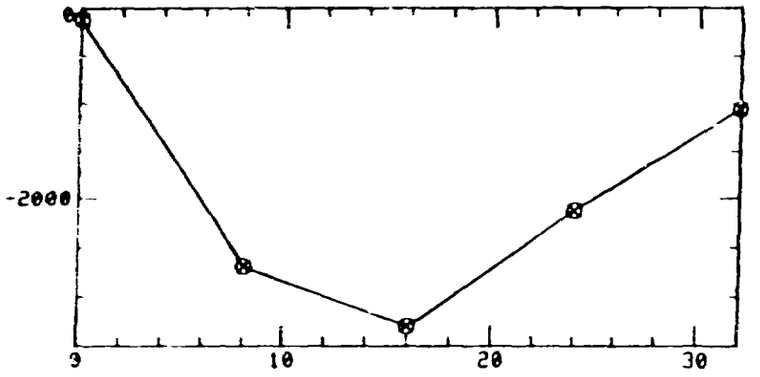

B_{tor} (Gauss)

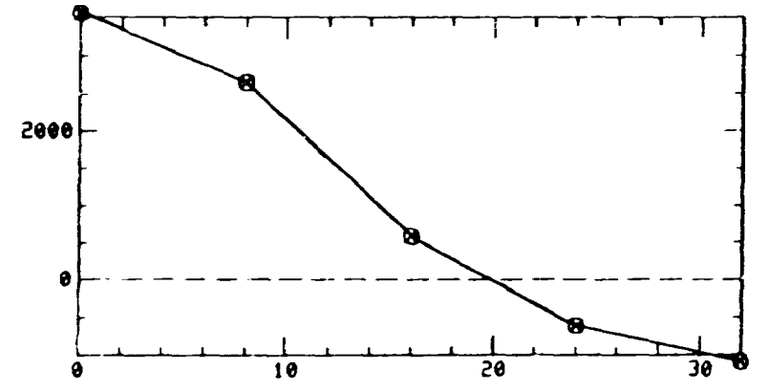

B_{pol} (Gauss)

RADIUS (cm)

t = 0·14 ms

Figure 9

KINKED Z-PINCH HELICITY SOURCE

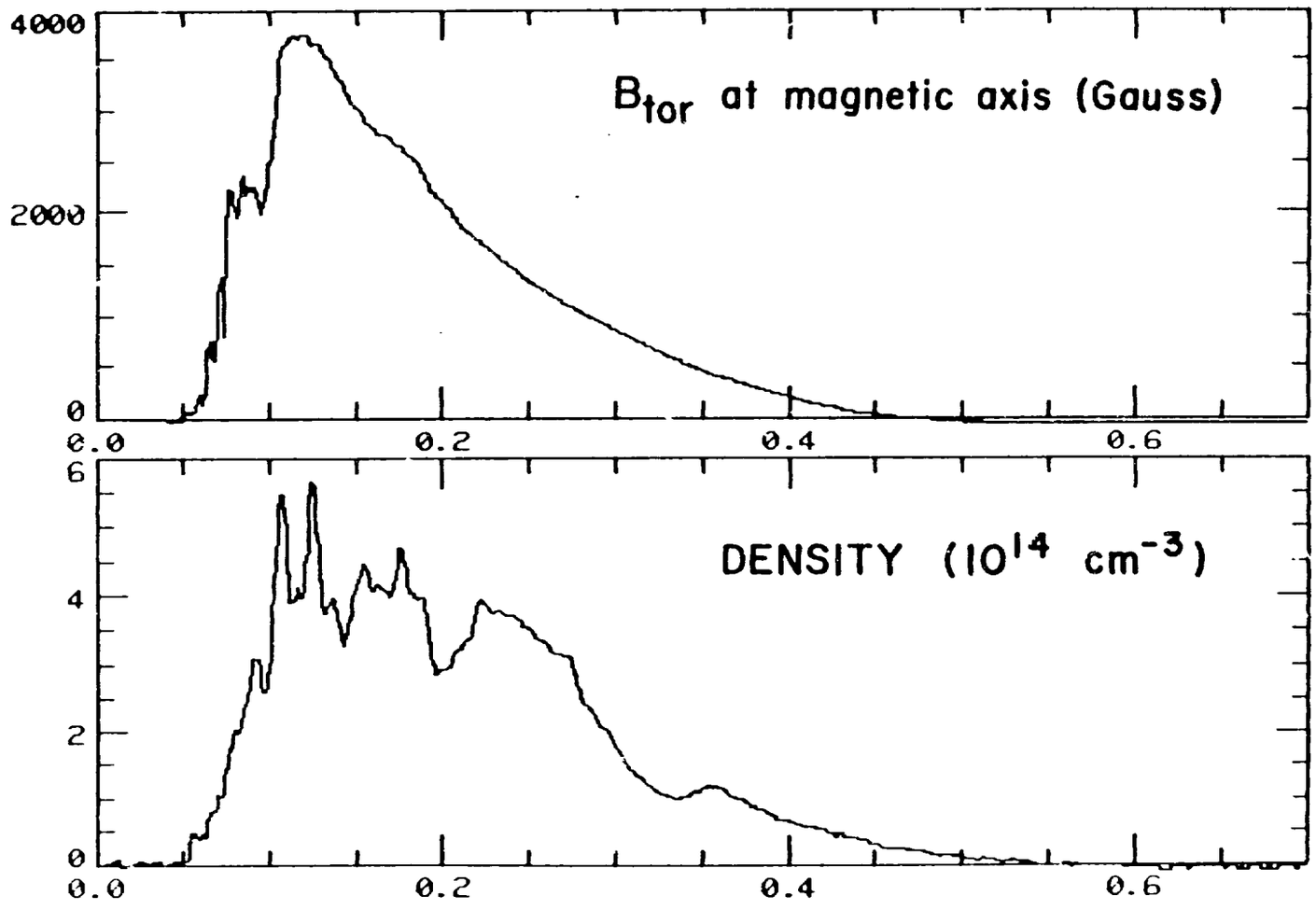

Figure 10